MODELLING OF THE SCATTERING BY A SMOOTH DIELECTRIC CYLINDER: STUDY OF THE COMPLEX SCATTERING MATRIX

L Thirion[1], C Dahon[2,3], A Lefevre[4], I Chênerie[1], L Ferro-Famil[2], C Titin-Schnaider[3]

[1] *AD2M, Université Paul Sabatier, 118 route de Narbonne, 31062 Toulouse, France, Email: thirion@cict.fr, chenerie@cict.fr*
[2] *Laboratoire Antennes Radar Telecom, Université de Rennes 1, 263 Avenue General Leclerc, 35042 Rennes, France, Email: cyril.dahon@onera.fr, Laurent.Ferro-Famil@univ-rennes1.fr*
[3] *IRSAMC, Université Paul Sabatier, 118 route de Narbonne, 31062 Toulouse, France, Email: lefevre@irsamc.ups-tlse.fr*
[4] *ONERA-PALAISEAU, DEMR/TSI Chemin de la Huniere, 91761 Palaiseau, France, Email: titin-schneider@onera.fr*

ABSTRACT

The interpretation of SAR data remains particularly difficult in the case of forests. Interferometric or/and polarimetric studies may enable us to retrieve some characteristics of the forest and identify the relevant scattering mechanisms involved in the global scattering phenomenon. A lot of numerical models have been developed to make the retrieval of such complex scenes easier. Both interferometry and polarimetry require a good knowledge of the scattering matrix, which is studied here for a single scatterer with a focusing on trunks, branches and needles, which are generally modelled by cylinders. The scattering matrix is simulated with two different commonly used models, based on semi-exact computations. The complex scattering matrix is computed for several local mechanisms involved in the global scattering by forested areas. Significantly results are found, pointing out that such studies are necessary before focusing on forest scattering modelling.

1 INTRODUCTION

Models of forest scattering involve two kinds of scatterers: branches and leaves, which are usually modelled by respectively dielectric flat ellipsoids and cylinders. In many of these models, the field scattered from cylinders is obtained by semi-exact computations involving the infinite cylinder approximation, which consists in replacing the field inside the cylinder by the field inside the same cylinder, but with infinite length [1,2,3]. This approximation leads to two non-equivalent formulation. Here, we will study the scattering matrix and the polarimetric parameters (SPAN, C and α), computed within these two formulations for three characteristic mechanisms involved in the modelling of a whole forest. We will comment the approximations made and raise some differences between the computations that may lead to different polarimetric interpretations for the same configuration.

2 COMPUTATION OF THE SCATTERED FIELD

Here, we will sketch the derivation of the field scattered by a cylinder of finite length h, permittivity ε and radius a, by using two different integral representations. The incident wave is of the form $\mathbf{E}_i(\mathbf{r}) = \mathbf{E}_0\, e^{-jk_0\mathbf{i}.\mathbf{r}+j\omega t}$, where $\mathbf{i}$ is the incident direction and $\mathbf{s}$ the scattering direction. Hence the field scattered by the cylinder in far zone may be expressed through the 2×2 scattering matrix $\mathbf{S}$: $\mathbf{E}_s(\mathbf{r}) = \frac{e^{-jk_0|\mathbf{r}|}}{|\mathbf{r}|}\mathbf{S}.\mathbf{E}_i$

2.1 Volume integral formulation

The scattered field can be expressed by solving the vector Helmholtz equation, which in far zone simply gives:

$$\mathbf{E}_s = \frac{(\varepsilon_r - 1)k_0^2}{4\pi r}\, e^{-jk_0 r}(\mathbf{I} - \mathbf{ss}) \int_V dv'\, \mathbf{E}_{in}(\mathbf{r}')e^{jk_0\mathbf{s}.\mathbf{r}'} \tag{1}$$

where $\mathbf{I}$ is the 3×3 identity tensor. In order to compute (1), we will use the infinite cylinder approximation. The final form of the scattered field may be found in [1].

2.2 Surface currents formulation

The derivation from Eq. (3) is not restricted to the scattering by a cylinder. Equivalent to this derivation is the derivation trough the surface equivalent currents, which, for a scatterer distributed in volume V of surface ∂V, can be written as:

$$
\begin{aligned}
\mathbf{E}_s(\mathbf{r}) &= -\nabla\times\nabla\times\frac{j\eta_0}{4\pi k_0}\int_{\partial V} ds'\,\mathbf{n}'\times(\mathbf{H}_i(\mathbf{r}')+\mathbf{H}_s(\mathbf{r}'))G_0(\mathbf{r}-\mathbf{r}') \\
&+ \nabla\times\frac{1}{4\pi}\int_{\partial V} ds'\,\mathbf{n}'\times(\mathbf{E}_i(\mathbf{r}')+\mathbf{E}_s(\mathbf{r}'))G_0(\mathbf{r}-\mathbf{r}') \\
\mathbf{H}_s(\mathbf{r}) &= +\frac{j\eta_0^{-1}}{4\pi k_0}\nabla\times\nabla\times\int_{\partial V} ds'\,\mathbf{n}'\times(\mathbf{E}_i(\mathbf{r}')+\mathbf{E}_s(\mathbf{r}'))G_0(\mathbf{r}-\mathbf{r}') \\
&+ \frac{1}{4\pi}\nabla\times\int_{\partial V} ds'\,\mathbf{n}'\times(\mathbf{H}_i(\mathbf{r}')+\mathbf{H}_s(\mathbf{r}'))G_0(\mathbf{r}-\mathbf{r}')
\end{aligned}
\tag{2}
$$

In the case of a thin cylinder, we will use the infinite cylinder approximation again. In addition, instead of integrating over the whole surface of the cylinder in Eq. (3), we will integrate over the lateral surface, ignoring the effect of the end caps. The final form of the scattered field obtained with this formulation may be found in [4].

2.3 Discussion of the two formulations

The difference between the two computations is twofold. First, the volume and surface (with the whole surface of the finite cylinder) integral formulations are not equivalent since the field of the infinite cylinder do not respect the good boundary conditions. Second, as explained above, the computation through the surface currents only takes into account lateral currents and then ignores the end caps, which is not the case for the volume integral computation. Hence, we expect that the former computation will be more relevant to describing the field scattered by a cylinder included in a system such that it is prolongated by other scatterers located at its end caps. This is typically the case of a branch in a tree, which is generally located between two other branches, such that the currents at the end caps are very few deformed. At the opposite, the latter computation seems more relevant to describing isolated cylinders, like truncated trunks, for example. We then expect the two computations to be more different at rather low incidence and high frequency (or large cylinder).

3 COMPARISON OF THE FORMULATIONS

In this paper, a study is proposed, consisting in comparing the two modelling when applied to usual cases such as backscattering, forward and specular scattering. We aim at evaluating how different these models are and the consequences on simulations. In order to proceed to this study, a default case is defined with moisture $m = 0.43$, incidence angle $\theta_i = 35°$ and Eulerian angles $\alpha = \beta = 0°$. Three frequencies are considered, corresponding to P Band (0.44 GHz), L Band (1.3 GHz) and C-Band (5.3 GHz). Three sizes of cylinder are chosen in order to test the two models on elements comparable with trunks or small branches.

3.1 Backscattering coefficient

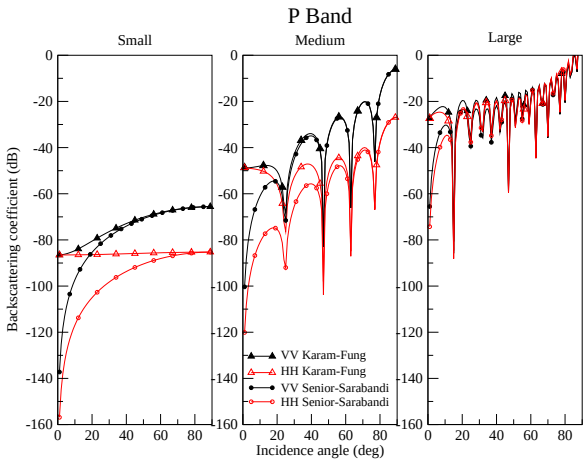

Figure 1: Comparisons of CEO polarised backscattering coefficients of a cylinder versus the incidence angle, under infinite cylinder approximation following Senior-Sarabandi or Karam-Fung calculations.

In Fig. 1, it is possible to compare at P Band the backscattering responses of the same cylinders - small ($a = 0.2$ cm, $h = 10$ cm), medium ($a = 1.5$ cm, $h = 1.5$ m) or large ($a = 20$ cm, $h = 6$ m) - considered either with Karam and Fung's (Ka-Fu) formulation or with Senior and Sarabandi's (Se-Sa) one.

We observe that the former is always above the latter. Both give the same results at normal incidence and the difference increases when the incidence angle decreases, the effect of the end caps being more important at low incidence. In addition, this difference is more visible for HH-polarisation. However, it is reduced by the increasing of the radius or the frequency. For long cylinders or high frequency, the backscattering coefficient is very sensitive to variations of the incidence angle (or equivalently the orientation of the axis), which implies to have good precision on ground truth data.

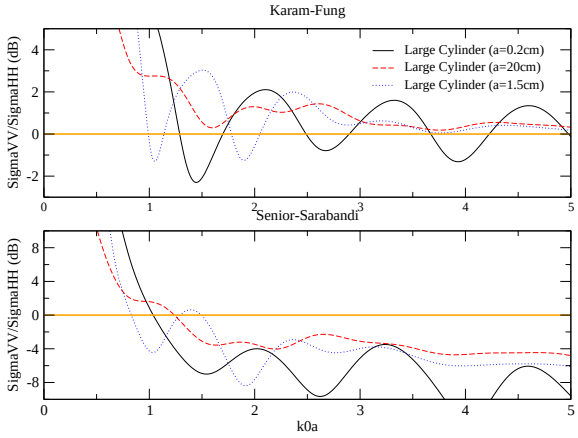

Figure 2: Comparisons of co polarised backscattering coefficients of a cylinder versus the wave number, under infinite cylinder approximation following Senior-Sarabandi or Karam-Fung calculations for different radii.

The ratio of co-polarised backscattering coefficients is plotted (in dB) in Fig. (2) versus the wave number for a large cylinder at an incidence angle of $35°$ and for different radii, exhibiting strong differences between the models. Sign inversions appear at high frequency, that is $\lambda \lesssim 10a$.

3.2 Forward scattering

The forward scattering theorem relates the attenuation of the incident wave to the imaginary part of the scattering matrix in the forward direction.

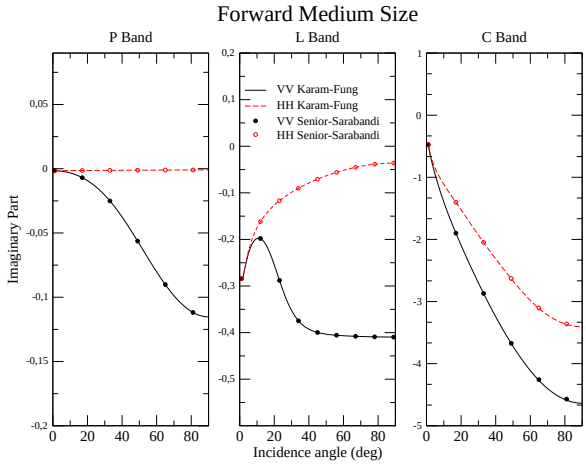

Figure 3: Comparisons of forward scattering imaginary part of a medium size cylinder versus the incidence angle, under infinite cylinder approximation following Senior-Sarabandi or Karam-Fung calculations at P-, L- and C- Bands.

In Fig. 3 simulations at P- and L- Bands are displayed. As expected, the attenuation depends strongly on incidence angle and on frequency. Both formulations give the same results, except for very high frequencies (not displayed here). However, we expect that the infinite cylinder approximation is not valid at very high frequency, where the sign inversions met above occur.

In addition, these variations are non monotonous, making the interpretation difficult and further studies necessary in order to understand this behavior.

3.3 Specular scattering

Specular scattering is an example of an event taking part in a double scattering mechanism in a forest. In Fig. 4, the specular scattering coefficient is plotted versus the incidence angle for different sizes of cylinder and for different frequencies. Here again a difference between surface and volume formulations appears at high frequency, when $\lambda \sim 10a$. We can see in Fig. 4 that the scattering coefficient increases with the radius. In addition, we notice that the VV-polarisation starts to dominate near after its minimum, which is reminiscent of the Brewster angle.

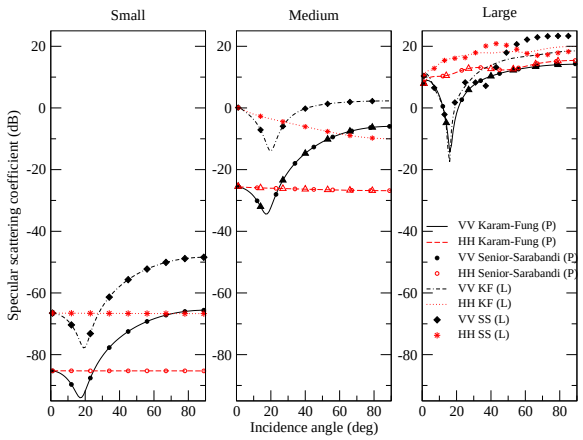

Figure 4: Comparisons of specular scattering coefficient of different cylinders versus the incidence angle, under infinite cylinder approximation following Senior-Sarabandi or Karam-Fung calculations at P- and L- Bands.

4 POLARIMETRIC STUDY

In this section, we will study the three characteristic scattering mechanisms of the previous section through polarimetric parameters. Each of the last two mechanisms will be combined with a perfect conducting plane to get a monostatic like configuration.

4.1 SPAN

The SPAN is the scattered power contained in the four polarimetric channels and is defined by SPAN $= \mathrm{Tr}\,\mathbf{S}\mathbf{S}^*$.

In Fig. 5 is shown the Span for a medium cylinder with moisture ratio $m = 0.43$. It can be seen that the forward SPAN dominates the specular one, the backscattering SPAN being very small except near normal incidence where it reaches the specular SPAN level. In addition, the higher the frequency, the more the forward SPAN dominates (the same behaviour, not shown here, is observed when increasing the moisture ratio).

We conclude that the forward and the specular scattering mechanisms are the most important ones and that their contributions are preponderant for large cylinders such as trunks or big branches. Backscattering mechanism has to be taken into account when the local incidence angle is near from $90°$, which in a forest can appear when a cylinder is used to model a branch.

4.2 The α polarimetric parameter

A coherency matrix $\mathbf{T}$ is obtained by performing a correlation product $< \mathbf{T} >=< \overrightarrow{k} \cdot \overrightarrow{k}^{t*} >$ between two target vectors

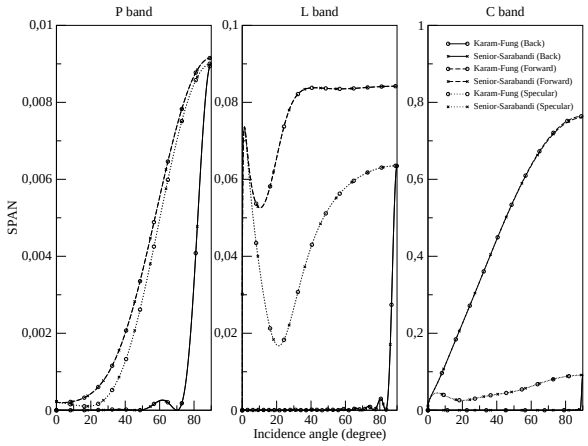

Figure 5: SPAN versus incidence angle for three frequency bands and the three main mechanisms.

$\overrightarrow{k}$ depending on scattering matrix elements such as:

$$\overrightarrow{k} = \frac{1}{\sqrt{2}} \cdot [S_{hh} + S_{vv}, S_{hh} - S_{vv}, 2S_{hv}]^t \tag{3}$$

The α parameter is extracted from the $\mathbf{T}$ coherency matrix eigenvectors [5]. It is valid in a deterministic or random configuration. A value of α smaller (resp. larger) than $45°$ indicates a single bounce (resp. double bounce).

In this study, the two different models fit rarely in backscattering because it is strongly dependent on the cylinder end caps.

4.2.a Analysis

In Fig. 6 is plotted the α parameter obtained for a medium size cylinder versus the incidence angle θ. For the backscattering and the forward scattering, α increases with. The maximum level is obtained for grazing incidences. In backscattering, this maximum can make $\alpha > 45°$ if λ is not large enough compared to a. Hence, in the L-band configuration, it is either a realistic behaviour more difficult to inverse or a frequency limitation which excludes big trunks modeling. The forward scattering has a single bounce signature. In specular scattering, α indicates a single bounce at low incidence angles and a double bounce at high ones. The frequency limitation can be seen too. Therefore, the double bounce α signature depends on the scatterer and radar configuration.
In the low frequency domain ($\alpha \lesssim a$), it has been observed that α has a monotonous increase with an increasing moisture ratio except for the specular scattering where it decreases after a maximal value (not displayed here).
For an increasing β orientation angle, α increases until its maximum for $\beta = 90°$ in the forward and backscattering configurations. Both mechanisms are less and less detected as single bounce when the cylinder becomes more horizontal. This maximum can exceed $45°$ in backscattering if $\lambda \lesssim a$ (not displayed here). The specular scattering is seen as a double bounce for a vertical cylinder and as a single bounce for a horizontal one. The orientation information has to be known before to discriminate the different mechanisms.

4.2.b Discussion

In backscattering, the α interpretation has no ambiguity only if $\lambda \gg a$. A general threshold must be found to allow a coupled use of a low frequency model for the branches with a high frequency one for the trunks.
For the forward and the backscattering, α is a monotonous function of the physical parameters for $\lambda \gg a$ hence, inversion seems relatively easy. On the contrary the specular scattering α signature has not such a monotonous behaviour which renders the inversion more difficult.
The forward scattering is detected as a single bounce mechanism even if the cylinder scattering is reflected by a conducting plane. So, α can not distinguish forward and backscattering.
Some other polarimetric parameters may help to inverse and make the distinction between the two mechanisms.

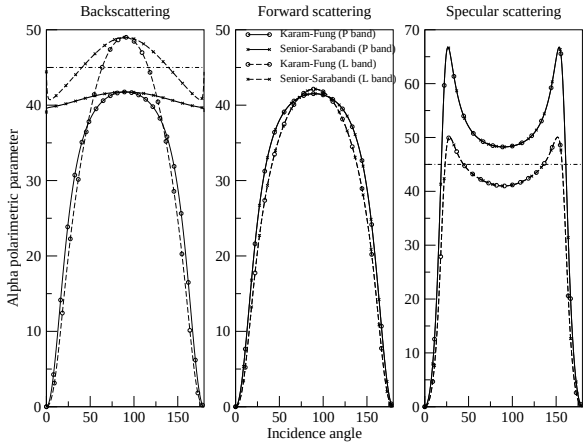

Figure 6: α polarimetric parameter versus incidence angle θ

5 CONCLUSION

In this communication, SER and polarimetric studies of scattering by single branches and trunks from two similar models have revealed a singular behaviour at large frequency, typically $\lambda < 10a$. This may be attributed to non trivial effects occurring in the scattering mechanisms or more probably to a frequency limitation of the infinite cylinder approximation. Hence, a high frequency formulation, such as from physical optics approximation is needed to describe large branches and trunks.

In addition, it has been found generically that the two formulations studied here differ around backscattering configurations, the more, the grazer the incidence. Hence, the effect of the presence of end caps or not is important in backscattering, and one has to be careful when choosing one of the formulations when the backscattering contribution is dominant.

The SPAN study led to a hierarchy between the three main mechanisms. It has been pointed out that the parameter α is not able to discriminate between back and forward scattering. However, its monotonous behaviour at not too high frequency indicates that it could be useful for inversion, when combined with other polarimetric parameters.

The study of this communication was focused on single scatterers. Such a study remains to be done on a collection of scatterers, "typical" of the ones used in modelling forested areas, by using both interferometric and polarimetric methods. The behaviour of the polarimetric parameters when varying the incidence direction and the distribution of the scatterers would be important to understanding how polarimetric signatures evolve when going from a single scatterer to a collection.

6 REFERENCES

1. **Karam M. A. and Fung A. K.** *Electromagnetic wave scattering from some vegetation samples***, IEEE Trans. Geosci. Remote Sensing, Vol. 26, 799-807, 1988**

2. **Karam M. A. and Fung A. K.** *Electromagnetic scattering from a layer of finite length, randomly oriented, dielectric, circular cylinders over a rough interface with application to vegetation***, Int. J. Remote Sensing, Vol. 9, 1109-34, 1988**

3. **Senior T. and Sarabandi K.** *Scattering models for point targets, in Radar Polarimetry for Geoscience Applications***, Artech House, Ed. Ulaby F. T and Elachi C., 1990**

4. **Lin Y. C. and Sarabandi K.** *Electromagnetic scattering model for a tree trunk above a tilted ground plane***, IEEE Trans. Geosci. Remote Sensing, Vol. 33, 1063-70**

5. **Cloude S. R., Pottier E.** *An entropy based classification scheme for land applications of polarimetric SAR***, IEEE Trans. Geosci. Remote Sensing, Vol. 35, 68-78, 1997.**